Lab on a Chip

Devices and applications at the micro- and nanoscale

Accepted Manuscript

This article can be cited before page numbers have been issued, to do this please use: E. B. Ko, T. Hu, Y. Zhang, X. Wang, Y. Song and C. Xu, *Lab Chip*, 2026, DOI: 10.1039/D6LC00230G.

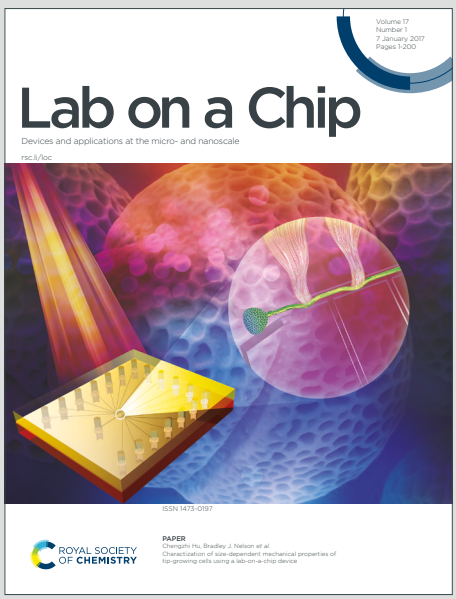

This is an Accepted Manuscript, which has been through the Royal Society of Chemistry peer review process and has been accepted for publication.

Accepted Manuscripts are published online shortly after acceptance, before technical editing, formatting and proof reading. Using this free service, authors can make their results available to the community, in citable form, before we publish the edited article. We will replace this Accepted Manuscript with the edited and formatted Advance Article as soon as it is available.

You can find more information about Accepted Manuscripts in the Information for Authors.

Please note that technical editing may introduce minor changes to the text and/or graphics, which may alter content. The journal's standard Terms & Conditions and the Ethical guidelines still apply. In no event shall the Royal Society of Chemistry be held responsible for any errors or omissions in this Accepted Manuscript or any consequences arising from the use of any information it contains.

View Article Online
DOI: 10.1039/D6LC00230G

Porous microneedle-based electrochemical aptamer biosensor for collection and quantitative analysis of dry eye disease biomarkers

Eira Beryle Ko#, Tianli Hu#, Ya Zhang, Xueyan Wang, Yu Song*, Chenjie Xu*

a. Department of Biomedical Engineering, College of Biomedicine, City University of Hong Kong, 83 Tat Chee Avenue, Kowloon Tong, Hong Kong SAR, P. R. China

#These authors contributed equally

*Correspondence: yusong@cityu.edu.hk (Y.S.), chenjie.xu@cityu.edu.hk (C.X.)

View Article Online
DOI: 10.1039/D6LC00230G

Abstract

Dry eye disease (DED) is a prevalent ocular disorder driven by tear film instability and inflammation. The quantitative measurement of molecular biomarkers in tears can provide a reliable, and accurate diagnosis and management of DED. This article introduces a porous microneedle-assisted electrochemical aptamer biosensor for the collection and quantitative analysis of DED-associated biomarkers in tear. The porous microneedle component collects tear while the electrochemical aptamer sensor detects interferon-gamma (IFN-γ), tumor necrosis factor-alpha (TNF-α), or matrix metalloproteinase-9 (MMP-9) with the detection limit of 4.46 pg/mL, 1.56 pg/mL, and 4.97 ng/mL, respectively. Clinically, DED is associated with 13 pg/mL of IFN-γ, 4 pg/mL of TNF-α, and MMP-9 concentrations of more than 40 ng/mL in tears, which are above the detection limits of our sensors. By taking MMP-9 as a model biomarker, we demonstrate a complete collection-to-detection workflow using this microneedle-aptamer biosensing device, which would facilitate the realization of point-of-care monitoring of DED.

Keywords: dry eye disease, microneedle, aptamer sensor, eye, tear

View Article Online
DOI: 10.1039/D6LC00230G

1. Introduction

Dry eye disease (DED) is a common ocular disorder characterized by tear film instability and symptoms such as ocular discomfort, photophobia, and visual disturbance.[1] Owing to lifestyle changes associated with prolonged screen use, there is an increasing global prevalence of DED, with an estimated 10-20% in the population of over the age of 40, and 5.5-23.1% in children.[2,3] Current diagnosis of DED relies on laborious tests such as slit-lamp examination, fluorescein staining, and tear film breakup time. Even the most accessible method, the Schirmer's test, measures only tear volume and correlates poorly with disease severity, limiting its value for DED grading or monitoring.

In 2017, Tear Film and Ocular Surface Society, Dry Eye WorkShop II reached consensus upon the vicious circle of inflammation-driven tear film abnormalities.[1] Clinical results show that DED leads to ocular inflammation and subsequently elevated secretion of molecules like lactoferrin, matrix metalloproteinase-9 (MMP-9), interleukin-6 (IL-6), interferon-gamma (IFN-γ), tumor necrosis factor-alpha (TNF-α).[4] The levels of these biomolecules can indicate normal or pathogenic processes and the response to a therapeutic intervention. This provides a great opportunity for researchers to pursue the point-of-care (POC) of DED by quantifying these biomolecules (biomarkers) with portable devices. For example, Lu et al. developed a silicon nanowire immunosensor for the quantitative detection of MMP-9, demonstrating the feasibility of miniaturized antibody-based assays.[5] Wang et al developed an aptamer-based biosensor that specifically recognized TNF-α with a detection limit of 0.34 pM in undiluted artificial tears.[6] The scientific exploration has led to the commercialization of devices like InflammaDry®.

Despite these exciting advancements, most diagnostic methods still require professional medical staff and additional tear-sampling tools such as glass capillary tubes or Schirmer's strips.

View Article Online
DOI: 10.1039/D6LC00230G

For example, in the InflammaDry® test, a medical professional has to collect tears from the patient's eye by placing a fleece in the lower palpebral conjunctiva.[7] This often leads to sample loss, biomarker retention, and ocular irritation, while also complicating the overall workflow. It also limits the practicality of DED self-assessment.

To address this overlooked issue, we introduce a microneedle (MN)-based biosensor to achieve a collection-to-detection workflow (Figure 1). The system is composed of a porous MN array for tear sampling and an aptamer-functionalized electrochemical sensor for downstream biomarker detection. The MN array, as reported in our previous work, is soft and light in weight, with anisotropic pores that mimic the structure of xylem.[8] This unique structure enables rapid tear extraction through the aligned microchannels while enabling high biomarker recovery ratio. In comparison to tear strips, the MNs were able to extract around the same volume of tears in only half the time in rats. In addition, the percentage of IFN-γ recovered from the porous MNs were much higher compared to that of tear strips, cotton swabs, and rayon swabs (89.7% ± 13.8%).[8] Aptamer is chosen as the recognition component because of its specificity, chemical stability, and cost effectiveness. We fabricate L-shaped gold (Au)-leaf-based electrodes and modify the Au working electrode (WE) with aptamers specific to DED tear biomarkers (i.e. IFN-γ, TNF-α, and MMP-9). The optimization of aptamer density on WE surface provides sensors with strong analytical performance, including well-defined calibration behavior, low detection limits, and high selectivity, good anti-interference in the presence of common tear components. Later, we integrate the MMP-9 aptamer sensor with the MN array and carry an *in vitro* demonstration of the complete collection-to-detection workflow. All these findings demonstrate the potential of this disposable and integrated aptamer sensor for tear biomarker quantitative assessment and point-of-care monitoring of DED.

View Article Online
DOI: 10.1039/D6LC00230G

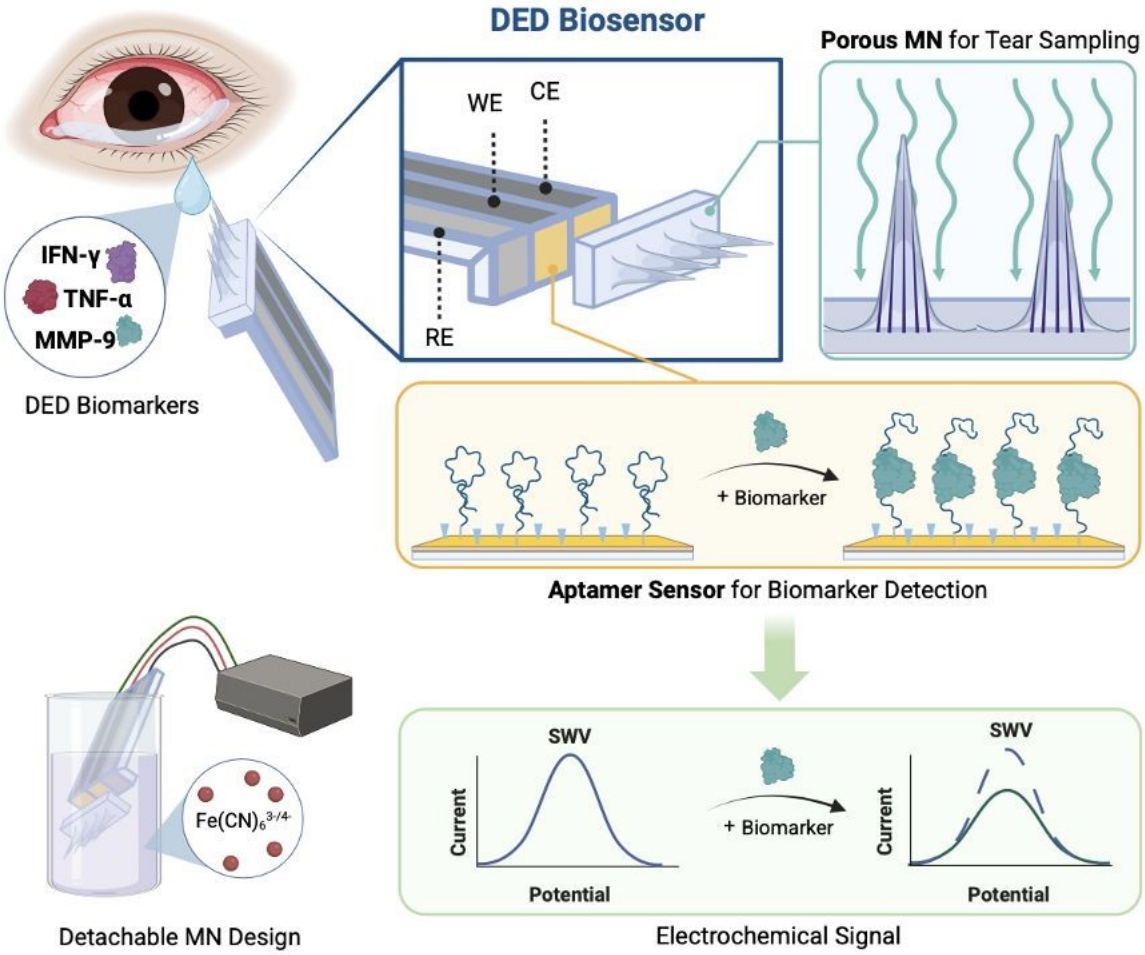

Figure 1. Schematic illustration of the porous MN-based electrochemical aptamer biosensing patch for tear collection and quantitative analysis of DED biomarkers.

2. Materials and Methods

Materials

Gold (Au) leaf and gold leaf adhesive were purchased from Nanjing Jin Bo Zhi Xiao Zhong Xin (China). Silver (Ag) and silver/ silver chloride (Ag/AgCl) paste were purchased from Shanghai Julong Electronic technology Co., Ltd (China). Artificial tear was purchased from the local

View Article Online
DOI: 10.1039/D6LC00230G

drugstore (Mentholatum, Hong Kong). Potassium ferricyanide ($K_3[Fe(CN)_6]$, potassium hexacyanoferrate (II) trihydrate ($K_4[Fe(CN)_6] \cdot 3H_2O$), potassium nitrate ($KNO_3$), potassium chloride (KCl), sodium chloride (NaCl), agarose, and glucose were purchased from J&K Scientific (China). Tris-(2-carboxyethyl) phosphine hydrochloride (TCEP) was purchased from Leyan (China). 4-(2-hydroxyethyl)-1-piperazineethanesulfonic acid (HEPES) was purchased from Thermo Fisher Scientific (USA). 6-mercapto-1-hexanol (MCH) was purchased from Sigma-Aldrich (USA). Recombinant human IFN-γ, TNF-α, and MMP-9 were purchased from BioLegend (USA). Human immunoglobulin E (IgE) protein was purchased from Abcam (USA). All aptamers were synthesized by BGI Genomics (China), and the sequence of each aptamer as follows:

IFN-γ-binding DNA aptamer: 5'-SH-C6-GGGGTTGGTTGTGTTGGGTGTTGTGTCCAACCC C-3';

TNF-α-binding RNA aptamer: 5'GGAGUAUCUGAUGACAAUUCGGAGCUCC-SH-C6-3';

MMP-9-binding DNA aptamer: 5′-SH-C6-TCGTATGGCACGGGGTTGGTGTTGGGTTGG-3′.

Electrochemical aptamer-based sensor fabrication

The fabrication began with 3D printing L-shaped polylactic acid (PLA) supports (7.5 mm length × 4 mm width and 7.5 mm length × 20 mm height, 1.75mm thickness) with two 0.5 mm wide indentations that ran along the entire surface. After applying gold leaf adhesive and drying at room temperature overnight, masking tape (0.5 mm width) was applied along the indentations as outlined on the L-shaped structure. Gold leaf (Au) was then affixed onto the support. Silver/silver chloride (Ag/AgCl) paste was applied on the entire reference electrode (RE), while Ag paste was applied only on the long side of the working and counter electrodes (WE and CE). The masking tape was carefully removed before curing in 75˚C for around 20 min until it dried. Around 2/3 of the electrode areas on the longer side with Ag and Ag/AgCl paste was covered with epoxy glue

View Article Online
DOI: 10.1039/D6LC00230G

for protection, leaving the ends exposed for electrochemical workstation connection. A three-electrode system was created after drying at room temperature for 12 h.

Before the addition of aptamers, Au electrodes were cleaned in a mild "piranha" solution with a 3:1 ratio of 50 mM sulphuric acid (H_2SO_4) and 25% w/v hydrogen peroxide (H_2O_2), followed by rinsing in deionized water and 75% ethanol.[9] The assembly of aptamers onto the Au WE was prepared according to the procedure outlined in the literature by Liu et al.[10] The aptamer solution was first heated to 95 ˚C for 10 min and gradually cooled to room temperature before use. Before immobilizing aptamers onto the WE, 0.02 M aptamer stock solution was reduced in 10 mM tris-(2-carboxyethyl) phosphine hydrochloride (TCEP) for 1 h. The thiolated aptamer solution was then diluted in 10 mM HEPES with 150 mM NaCl to the required concentrations of 1-5 μM. The WE was incubated in the aptamer solution at 4˚C for 16 h. The electrodes were then rinsed with deionized water, and 3 mM 6-mercapto-1-hexanol (MCH) was added to WE for 1 h. Finally, the electrodes were rinsed again and stored at 4˚C prior to use.

Morphological characterization of sensor by SEM and EDS

The surface of aptamer-modified WE before and after undergoing square wave voltammetry (SWV) measurement was imaged using field-emission scanning electron microscope (SEM) (FEI Quanta 250). Unmodified Au WE surface was analyzed with energy dispersive X-ray spectroscopy (EDS) on the same equipment.

Surface-enhanced Raman spectroscopy

Surface-enhanced Raman spectroscopy was done using WiTec Raman System at an excitation wavelength of 633 nm. A large area scan was carried out on the surface of the aptamer modified WE (20 × 20 μm) with 20 points per line, 20 lines per image, and an integration time of 3 s. The resulting data and images were processed using WiTec Project 5.1.

View Article Online
DOI: 10.1039/D6LC00230G

Sensor characterization

All electrochemical measurements were done with CHI 760E electrochemical analyzer workstation. All measurements were carried out in 5 mM ferri/ferrocyanide ($Fe(CN)_6^{3-/4-}$) buffer with 0.1 M potassium chloride (KCl) and 0.1 M potassium nitrate (KNO_3). Cyclic voltammetry (CV) was carried out from -1 V to 1 V, a scan rate of 0.1 V/s, and 10^{-4} A sensitivity on the same sensor before and after cleaning with mild "piranha" solution, after the addition of aptamer and after incubation in MCH. Electrochemical impedance spectroscopy (EIS) was completed as well for the same electrode modification steps on one sensor under the parameters of 0.1 to 100000 Hz and a 0.005 V amplitude. SWV at 60 Hz and 40mV amplitude over -0.05 V to 0.35 V was done on bare electrodes, as well as after aptamer-MCH modification and after addition of target biomarker on the same sensor.

Aptamer density optimization and sensor performance

We prepared sensors with different aptamer concentrations of 1, 3, and 5 μM. The sensors were first placed in 10 mM HEPES buffer with 150 mM NaCl for 15 min to equilibrate. The initial voltammogram was obtained via SWV in 5 mM ferricyanide buffer, with an amplitude of 40 mV at 60 Hz over -0.05 V to 0.35 V vs Ag/AgCl. The sensors were incubated with the target analytes under different concentrations in HEPES buffer for 15 min before performing SWV again with the same parameters. For human recombinant IFN-γ, 1, 5, 10, 15, and 20 pg/mL were used. For human recombinant TNF-α, 0.1, 0.5, 1, 5, and 10 pg/mL were prepared. As for human recombinant MMP-9, concentrations of 10, 20, 30, 40, and 50 ng/mL were tested. The same biomarker concentrations were used when measuring sensor performance. The resulting relative peak-current difference ($\Delta i/i_0$) were calculated based on the relative peak currents before (i_0) and after reacting with target (i_{target}) following the equation below.

View Article Online
DOI: 10.1039/D6LC00230G

$$\Delta i/i_0 = \frac{i_0 - i_{target}}{i_0}$$

Selectivity and anti-interference performance

We studied the SWV responses of IFN-γ sensors before and after reacting with 50 ng/mL IgE, 0.2 mM glucose, 10 pg/mL TNF-α, 40 ng/mL MMP-9, and 5 pg/mL IFN-γ in $Fe(CN)_6^{3-/4-}$. Similarly, TNF-α sensor responses before and after incubation in 50 ng/mL IgE, 0.2 mM glucose, 20 pg/mL IFN-γ, 40 ng/mL MMP-9, and 0.5 pg/mL TNF-α were compared. For MMP-9 sensors, the experiment was completed with 50 ng/mL IgE, 0.2 mM glucose, 20 pg/mL IFN-γ, 10 pg/mL TNF-α, and 20 ng/mL MMP-9. The anti-interference performance was measured through SWV after allowing each sensor to react in a solution with interfering molecules. The solution was prepared in HEPES with 50 ng/mL IgE, 0.2 mM glucose, 1 pg/mL IFN-γ, 0.1 pg/mL TNF-α, and 10 ng/mL MMP-9. The results ($\Delta i/i_0$) were then compared to that of the target marker only at the same concentration.

Repeatability

The SWV current without target was first collected after the fabrication of aptamer sensors. Each sensor was allowed to incubate with the target biomarker (5 pg/mL IFN-γ, 0.5 pg/mL TNF-α, or 20 ng/mL MMP-9) for 15 min before 3 consecutive SWV measurements. The repeatability was presented as the relative peak current difference ($\Delta i/i_0$) of the 3 consecutive measurements in each sensor.

Fabrication of MN patch

MN patches (1 x 10 array, with a tip length of 1000 μm) were fabricated following the procedure from our previous work.[8] In short, 10 μL of a prepolymer solution containing 5% wt gelatin and 1 M EDC/NHS were added into each PDMS-negative MN mold before centrifuging at 4000 rpm for 3 min to fill the tips. After filling up the rest of the mold (the base) with an additional 30 μL of the

View Article Online
DOI: 10.1039/D6LC00230G

prepolymer solution, they were cooled unidirectionally originating from the base in a cooling bath at -20 ˚C. The molds were subsequently left at -20 ˚C for 48 h and submerged in deionized water at room temperature for 16 h. After freeze-drying at -80 ˚C for 4 h and demolding, porous MN patches were obtained.

Morphological characterization of porous MN by SEM

The morphology of MN was imaged with field-emission scanning electron microscope (SEM) (FEI Quanta 250). The needles were cut and removed from the base, while the MN base was cut perpendicularly to reveal the internal structures. All samples were sputter coated with a 10-nm gold layer for SEM imaging.

Integration of MN with aptamer sensors for DED biomarker collection and detection in the hydrogel model

After the preparation of aptamer sensors, SWV measurements of each sensor was first recorded in $Fe(CN)_6^{3-/4-}$ as the baseline before integration with MN. To assemble the device, MN patch was attached on top of the aptamer sensor using 3M™ double-sided medical adhesive along the indentations in between the electrode areas (Figure 5A). We then set up a model system using 0.4% agarose gel.[11] 10 μL of artificial tears with various levels of recombinant human MMP-9 (10, 20, 30, 40, and 50 ng/mL) was added onto the agarose gel model to simulate healthy eye and dry eye (HE and DE). The artificial tears were then collected from the agarose gel model by placing the MN patch for approximately 3 min. The device was then left in $Fe(CN)_6^{3-/4-}$ buffer for 15 min before electrochemical measurements. The SWV results ($\Delta i/i_0$) were calculated based on the baseline SWV measurements recorded previously to obtain a standard curve.

View Article Online
DOI: 10.1039/D6LC00230G

Two individual samples of 20 ng/mL and 50 ng/mL of MMP-9 in artificial tears were prepared to represent HE tears and DE tears respectively. Using the integrated device, the artificial samples were recovered from the hydrogel model for SWV measurements in the same manner.

Statistical analysis

Each experiment was repeated at least 3 times. All data were shown as the means ± SD unless specified otherwise. Quantitative analysis was based on Welch's t-test to determine *p* values. In all cases, $p < 0.05$ was considered statistically significant (*$p < 0.05$, **$p < 0.01$, ***$p < 0.001$, n.s.: not significant).

3. Results and Discussion

3.1 Development of the electrochemical aptamer sensor

We developed an L-shaped electrochemical aptamer sensor as the biomarker detection module (Figure 2A). The L-shaped geometry provides mechanical support and enables the integration with the MN array during tear sampling. This L-shaped structure was 3D-printed using PLA, with indentations incorporated to spatially separate the electrodes, prevent electrical shorting, and reduce signal interference. The electrochemical electrodes were fabricated using Au leaf, Ag/AgCl paste, and Ag paste. Au leaf was first laminated onto the PLA substrate to define the regions of the WE, CE, and RE. Ag/AgCl paste was subsequently applied to the designated RE region to construct the Ag/AgCl reference electrode, while the Au-leaf-based WE and CE surfaces were retained as the active sensing interfaces. To stabilize conductivity and minimize side reactions during electrochemical measurements, the non-sensing areas of WE and CE were coated with Ag paste and sealed with epoxy. This ultimately provided a three-electrode system consisting of WE and CE against Ag/AgCl RE (Figure 2B). The use of 23 kt Au leaf, which has a purity of 95.8%,

View Article Online
DOI: 10.1039/D6LC00230G

in the fabrication of electrochemical sensor has been shown to exhibit similar electrochemical behaviour as commercial screen-printed electrodes.[12] The composition of the Au-leaf-based WE was verified through EDS. The electrode surface is mainly composed of Au (96.69 wt %), with only small traces of copper (Cu) and oxygen (O) that are generally present in commercial Au screen-printed electrodes [9,12] (Figure 2C).

The next step is to functionalize the Au WE with aptamer. Aptamer has been reported as the effective bioreceptor for inflammatory biomarkers, and its binding-induced conformational change can be transduced into electrochemical signals.[10] In the tears of patients with DED, IFN-γ level increases from ~4 pg/mL to ~13 pg/mL, TNF-α level rises from <0.5 pg/mL to ~4 pg/mL, and MMP-9 level exceeds 40 ng/mL.[4,13,14] Therefore, we synthesized thiolated aptamers with specificity to three biomarkers and immobilized them onto the Au WE *via* a standard thiol-based self-assembled monolayer formation process.[5,10,15] Briefly, aptamers with thiol modifications were first reduced in TCEP solution to cleave disulfide bonds, ensuring exposure of free thiol groups for Au binding. The aptamer solution was then diluted to the desired concentration of 1-5 μM in HEPES buffer and was casted on the surface of the WE for 16 h. After immobilization, MCH was added to the WE to passivate unoccupied Au sites and promote the formation of a well-packed sensing layer.

The modified electrode surface was characterized using Raman imaging (Figure 2D). Under 633 nm excitation, there were major peaks at 1340 and 1580 cm^{-1}, which are associated with the C-N and C=N stretching modes found in both adenine and guanine.[16] This confirms the presence of aptamers on the WE surface. Based on the quantitative signal at 1340 cm^{-1}, we could map the distribution of aptamers across the WE surface in both 2D and 3D (Figure 2E). In this case, 3 μM of MMP-9 aptamer on Au WE was mapped. It is expected that the distribution of

View Article Online
DOI: 10.1039/D6LC00230G

aptamers will appear denser with a higher aptamer density such as 5 μM, and more sparsely distributed on the surface with a lower aptamer density (e.g. 1 μM).

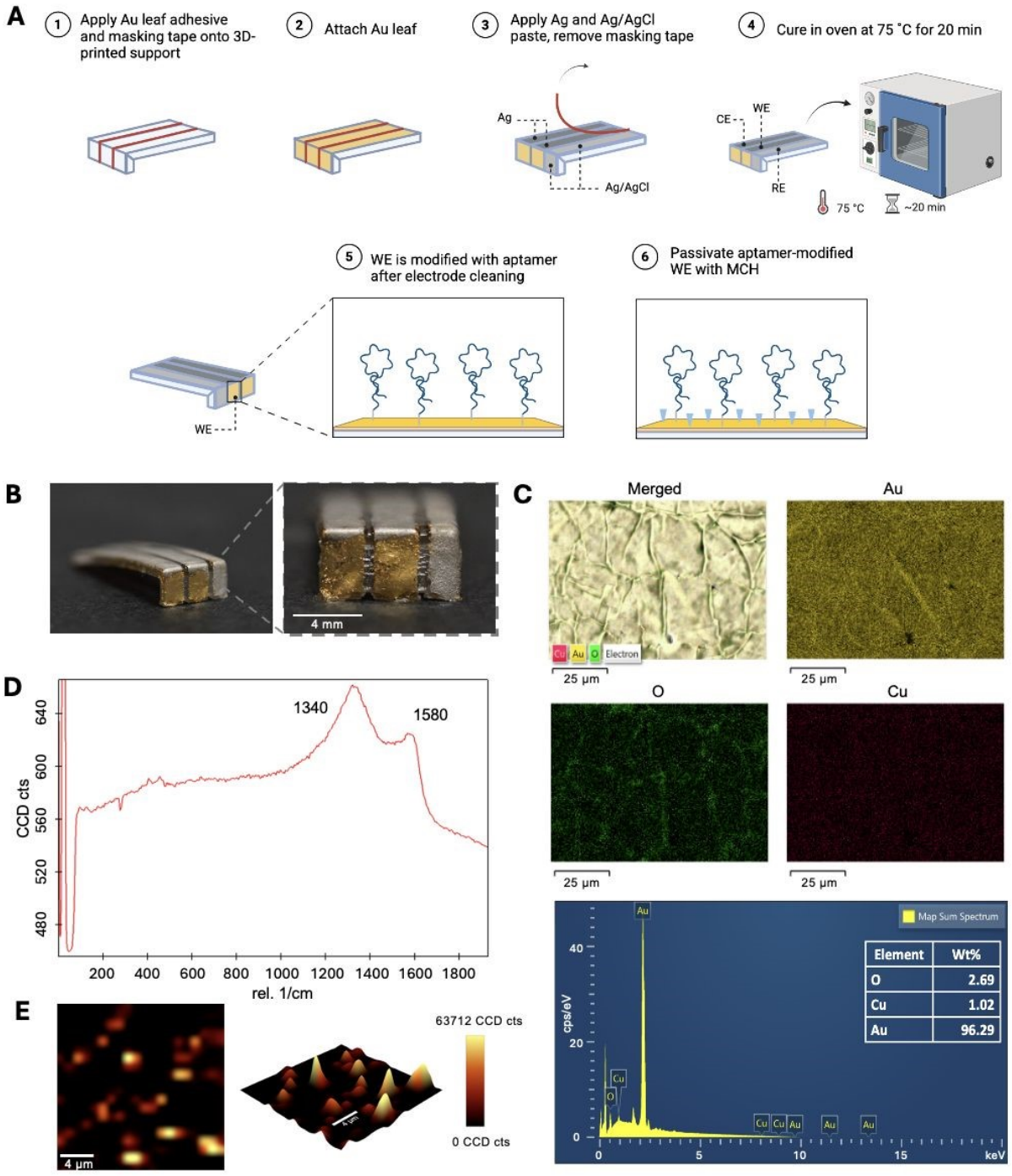

View Article Online
DOI: 10.1039/D6LC00230G

Figure 2. Development and surface characterization of the electrochemical aptamer sensor: (A) Schematic illustration of the fabrication process; (B) Images of the Au leaf electrodes, scale bar: 4 mm; (C) EDS of the bare Au WE; (D) Raman spectrum of aptamer modified WE; (E) 2D and 3D Raman mapping based on the intensity of 1340 cm^{-1} peak.

3.2 Electrochemical characterization of the functionalized electrode interface

We investigated how the formation of the aptamer/MCH monolayer modulated electron transfer at the electrode interface using the MMP-9 aptamer as an example. To confirm the stepwise surface modification on the WE, CV and EIS were performed in the buffer with 5 mM $Fe(CN)_6^{3-/4-}$, 0.1 M KCl and 0.1 M KNO_3, where the $Fe(CN)_6^{3-/4-}$ redox couple underwent reversible electron transfer interacting with the electrode surface (Figure 3A). In CV, the bare Au electrode exhibited high anodic peak currents at approximately 0.2 V due to rapid electron transfer. After electrode cleaning, the peak current increased compared to that of the bare Au electrode as surface resistance was reduced. Aptamer immobilization subsequently lowered the peak current, and additional current suppression was observed after MCH backfilling, which is consistent with increased interfacial resistance caused by the formation of a compact SAM (Figure 3B). Correspondingly, in the Nyquist plots, the straight lines at an angle for the bare Au WE and after cleaning reflected the low charge transfer resistance of the system. The slope became slightly steeper as surface resistance was lowered after electrode cleaning. Following aptamer immobilization, the graph displayed a semicircle trend, indicating a shift in surface chemistry and higher charge transfer resistance on the WE. The resistance was further increased with the formation of MCH monolayer as observed by the larger semicircle diameter (Figure 3C).

View Article Online
DOI: 10.1039/D6LC00230G

After validating the surface modification, SWV was used to verify the functionality of the aptamer-based sensing interface for DED biomarker detection. SWV responses with frequency of 60 Hz and an amplitude of 40 mV were recorded for the MMP-9 aptamer sensor after incubation with and without the target, 50 ng/mL of MMP-9 (Figure 3D). The voltage range was defined as -0.05 V to 0.35 V according to anodic peak position in the CV results (Figure 3B). A decrease in the SWV peak position from around 373 μA to 227 μA appeared after target binding, reflecting the slowed down electron-transfer process of the $Fe(CN)_6^{3-/4-}$ redox probe. When aptamers bind to their target analyte, the conformational change of aptamers would hinder the redox probes from interacting with the electrode surface, leading to a reduction in faradic current. These results collectively confirm that the ability of Au-leaf aptamer sensor in providing a stable functionalized interface and reliable electrochemical response for DED biomarker detection.

In addition, we examined the morphology of WE surface before and after electrochemical interrogation with the target analyte, MMP-9, using SEM (Figure S1). Though some folds and cracks existed on the WE surface from the Au leaf application during fabrication, no significant structural damage occurred during sensing process. Despite imperfections, the Au-leaf electrodes exhibited sufficient structural integrity and robustness for the use of a disposable and low-cost sensor.

3.3 Optimization of the aptamer density on sensing interface

We further optimized the aptamer concentration on the WE. Low aptamer coverage leads to insufficient target capture, whereas overly dense aptamer layer impedes electron transfer and reduces the dynamic signal window. The ideal aptamer density should produce the largest current decrease upon target binding. We functionalized WEs with 1, 3, or 5 μM of IFN-γ, TNF-α, and MMP-9 aptamers, and then measured their SWV responses in 5 mM $Fe(CN)_6^{3-/4-}$ buffer before

View Article Online
DOI: 10.1039/D6LC00230G

and after incubation with biomarker solutions spanning healthy and dry-eye tear levels (1-20 pg/mL IFN-γ, 0.1-10 pg/mL TNF-α, and 10-50 ng/mL MMP-9) (Figure S2). To quantitatively compare aptamer loadings, signal suppression was analyzed through the relative peak-current change ($\Delta i/i_0$), where i_0 is the initial current measured before target binding, and Δi is the difference in peak current before and after incubation with each biomarker solution (Figure 3E-G). Across all densities tested for each aptamer sensor, the difference in relative peak current increased progressively with increasing biomarker concentration, reflecting the enhanced electron-transfer blockage caused by aptamer-target binding. Among the concentrations tested, the overall trend showed that 3 μM of IFN-γ aptamer, 5 μM of TNF-α aptamer, and 3 μM of MMP-9 aptamer had the largest current suppression across their respective analyte ranges. Therefore, these aptamer concentrations provided the highest sensitivity and were applied in the subsequent experiments. Together, these results demonstrate that the optimization of aptamer surface density is critical for maximizing signal responsiveness and establishing a robust electrochemical sensing interface for DED tear biomarkers.

View Article Online
DOI: 10.1039/D6LC00230G

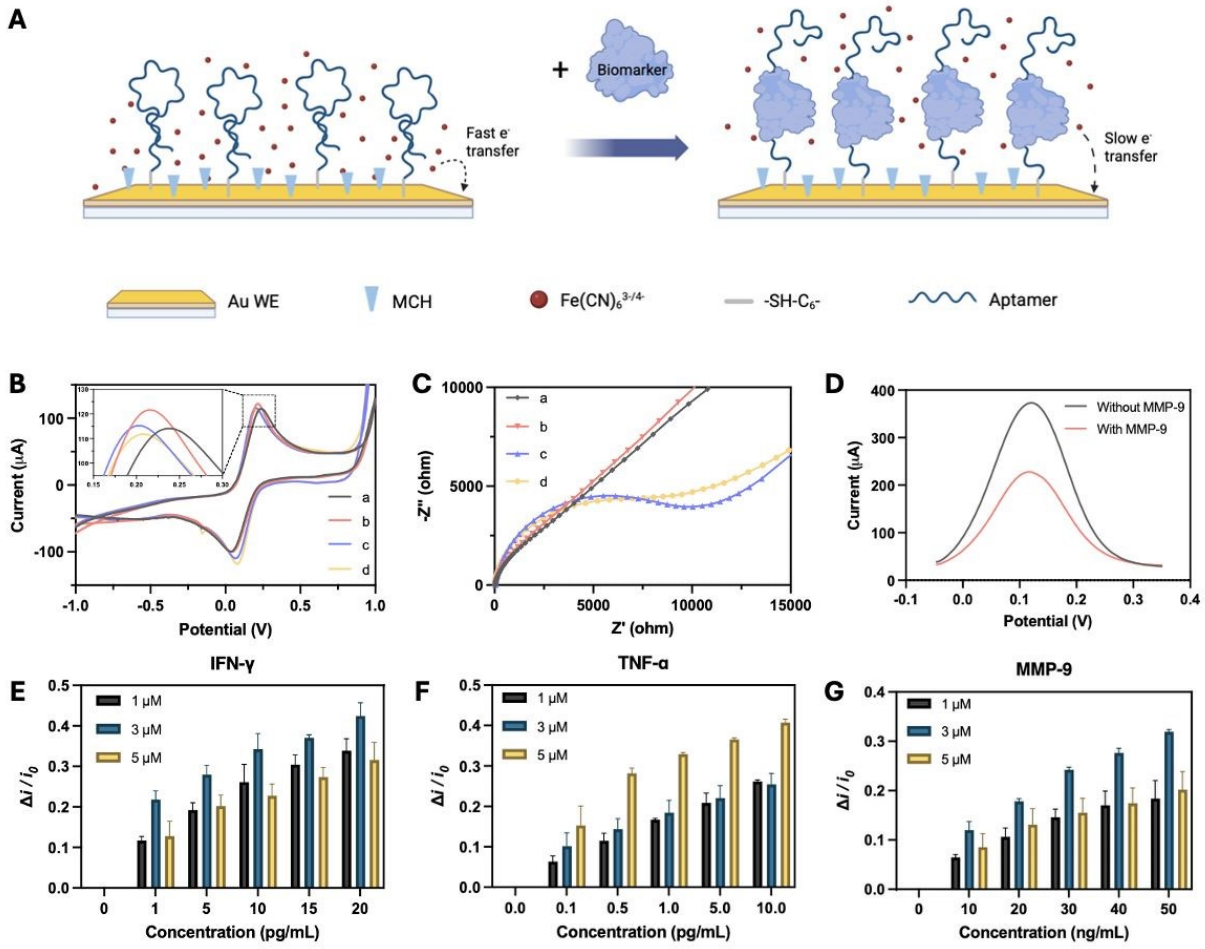

Figure 3. Electrochemical characterization and optimization of the electrochemical aptamer sensor: (A) working principle; (B) CV and (C) EIS of the electrode after each modification step, (a) bare Au WE, (b) Au WE after cleaning, (c) aptamer-functionalized WE, (d) aptamer/MCH-modified WE; (D) SWV responses of the MMP-9 aptamer sensor with and without 50 ng/mL MMP-9; (E) optimization of IFN-γ aptamer concentration (1, 3, and 5 μM), where the biomarker IFN-γ concentration changes from 0 to 20 pg/mL; (F) optimization of TNF-α aptamer concentration (1, 3, and 5 μM), where the biomarker TNF-α concentration changes from 0 to 10 pg/mL; (G) optimization of MMP-9 aptamer concentration (1, 3, and 5 μM), where the biomarker MMP-9 concentration changes from 0 to 50 ng/mL.

View Article Online
DOI: 10.1039/D6LC00230G

3.4 Analytical performance of the aptamer sensors

Based on the SWV responses of the optimal sensors (i.e. 3 μM of IFN-γ aptamer, 5 μM of TNF-α aptamer, and 3 μM of MMP-9 aptamer) when exposed to different target concentrations in 5 mM $Fe(CN)_6^{3-/4-}$ buffer (Figure 4A-C), the relationship between biomarker concentration (C) and relative peak-current differences ($\Delta i/i_0$) were reconstructed into calibration curves for analysis. The IFN-γ aptamer sensor exhibited a linear relationship where the calibration curve was fitted to a line with the equation: $\Delta i/i_0 = 0.01291*C_{IFN\text{-}\gamma} + 0.1196$, and an R^2 of 0.86 (Figure 4D). Similarly, the TNF-α sensor calibration curve displayed a linear regression with the equation: $\Delta i/i_0 = 0.12*[\log(C_{TNF\text{-}\alpha})] + 0.3008$, and an R^2 of 0.90 (Figure 4E). MMP-9 sensor was calibrated to a line of $\Delta i/i_0 = 0.004966*C_{MMP\text{-}9} + 0.07803$, and an R^2 of 0.97 (Figure 4F). The limit of detection (LOD) for each sensor was calculated based on the standard deviation and the slope of the calibration curve. The LODs of the IFN-γ, TNF-α, and MMP-9 sensors were 4.46 pg/mL, 1.56 pg/mL, and 4.97 ng/mL respectively. It should be noted that the LOD of TNF-α is higher the healthy levels of less than 0.5 pg/mL, causing limitations in the detection of subtle changes in healthy tears at low concentrations under the LOD. However, this LOD is sufficient for the monitoring of DED since it falls far below 4 pg/mL, which is the level that is indicative of DED. Because DED is an inflammatory disease, the TNF-α tear levels is expected to rise even further as the disease progresses. These results reflect that all three aptamer sensors provide sufficiently low LOD and broad dynamic ranges suitable for tear-based DED biomarker analysis.

To demonstrate the specificity, each sensor was challenged with individual non-specific tear component at concentrations representative of physiological tear backgrounds, including 50 ng/mL IgE, 0.2 mM glucose, 20 pg/mL IFN-γ, 10 pg/mL TNF-α, and 40 ng/mL MMP-9.[17,18] The

View Article Online
DOI: 10.1039/D6LC00230G

responses were then compared to the respective analyte of interest at a lower concentration, i.e. 5 pg/mL IFN-γ, 0.5 pg/mL TNF-α, or 20 ng/mL MMP-9. As shown in Figure 4G-I, all sensors displayed a specific response to the corresponding analytes as reflected by the greatest decrease in current compared to the other non-specific analytes, demonstrating their strong specificity. However, it was observed that in the presence of non-specific molecules, especially glucose, the sensors showed a negative response (i.e. and increase in current). This is potentially caused by the electrostatic interaction between the molecules and aptamers. In the case of glucose, it has been reported that the small molecule could interfere and increase electron transfer, leading to an increase in current. Meanwhile, other biomolecules could cause biofouling or reduced electrical repulsion due to their nature, generating a negative response.[17,18] Therefore, to further evaluate the sensing performance in more complex environments, the anti-interference performance of the sensors was investigated by incubating each target biomarker together with a mixture of all the non-specific tear components. The signal response was compared to that of only the target at the same concentration in HEPES buffer (Figure 4K-L). There was no significant difference between the two groups for all sensors, indicating that coexisting tear constituents do not impede target recognition or electron-transfer processes. While the effect of non-specific markers is limited in the current sensors, the application of nanostructure strategies could be explored to further improve aptamer sensor performance and minimize non-specific responses.[19]

View Article Online
DOI: 10.1039/D6LC00230G

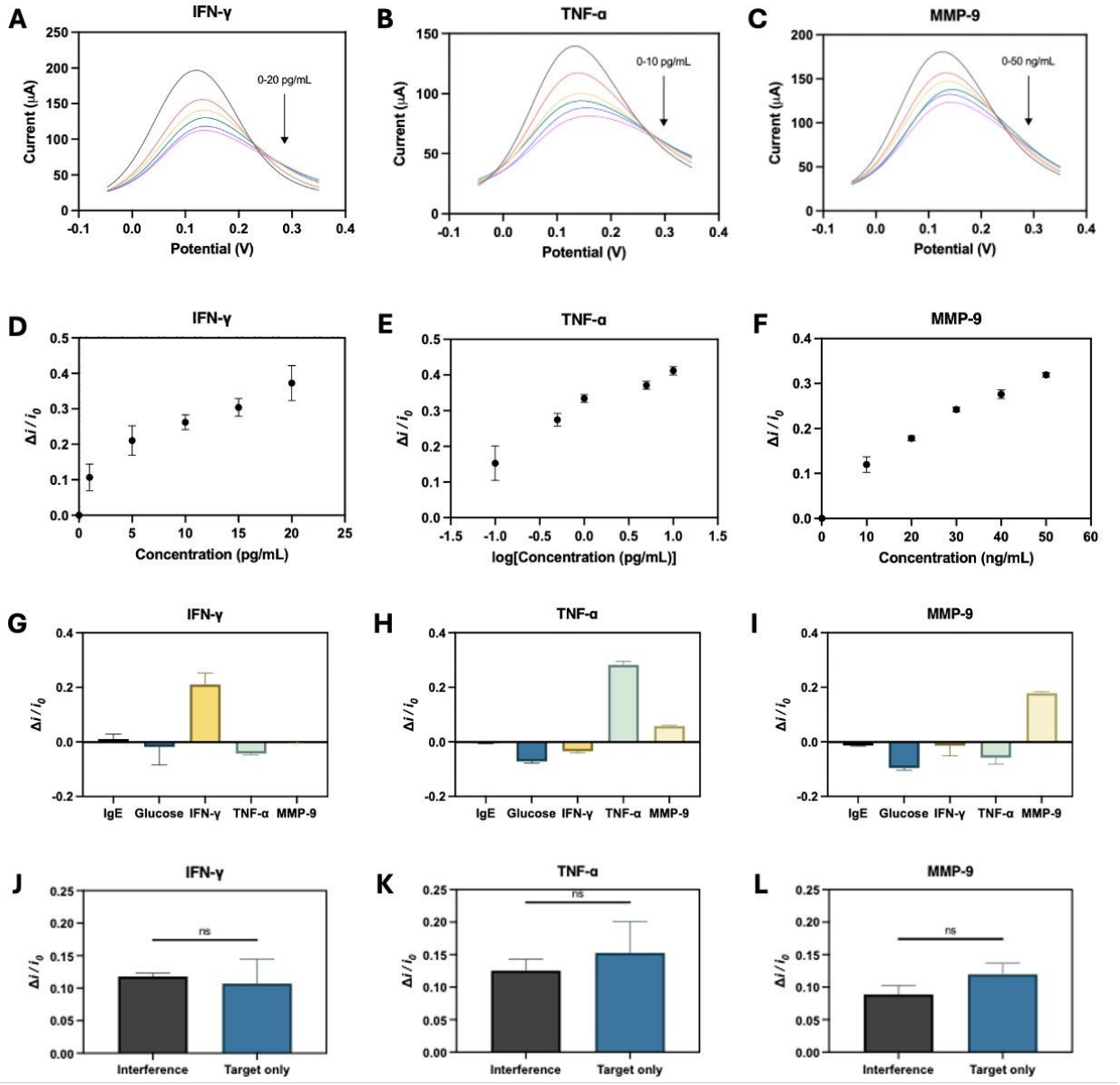

Figure 4. Characterization of the sensor sensitivity and selectivity: SWV responses of (A) IFN-γ sensor in 0-20 pg/mL IFN-γ, (B) TNF-α sensor in 0-10 pg/mL TNF-α, and (C) MMP-9 sensor in 0-50 ng/mL MMP-9; calibration curve of (D) IFN-γ sensor, (E) TNF-α sensor, (F) MMP-9 sensor; (G) Specificity of IFN-γ sensor to 50 ng/mL IgE, 0.2 mM glucose, 5 pg/mL IFN-γ, 10 pg/mL TNF-α, 40 ng/mL MMP-9; (H) Specificity of TNF-α sensor to 50 ng/mL IgE, 0.2 mM glucose, 20 pg/mL IFN-γ, 0.5 pg/mL TNF-α, 40 ng/mL MMP-9; (I) Specificity of MMP-9 sensor to 50 ng/mL IgE, 0.2 mM glucose, 20 pg/mL IFN-γ, 10 pg/mL TNF-α, and 20 ng/mL MMP-9; anti-interference

View Article Online
DOI: 10.1039/D6LC00230G

performance in interfering solution (50 ng/mL IgE, 0.2 mM glucose, 1 pg/mL IFN-γ, 0.1 pg/mL TNF-α, and 10 ng/mL MMP-9) of (J) IFN-γ sensor against 1 pg/mL IFN-γ, (K) TNF-α sensor against 0.1 pg/mL TNF-α, (L) MMP-9 sensor against 10 ng/mL MMP-9.

3.5 Reproducibility of aptamer sensors

The reproducibility of the Au leaf aptamer sensors was assessed (Figure S3). 3 of each aptamer sensor (IFN-γ, TNF-α, and MMP-9) were fabricated at the same time. After incubation with the same target analyte concentration (5 pg/mL IFN-γ, 0.5 pg/mL TNF-α, or 20 ng/mL MMP-9), 3 consecutive SWV measurements in $Fe(CN)_6^{3-/4-}$ buffer were completed for each individual sensor, obtaining 3 relative peak-current difference values. The means of the repeated responses were compared. Even at lower biomarker concentrations, each group was able to produce similar electrochemical responses. The results demonstrated the reproducibility of the IFN-γ, TNF-α, and MMP-9 aptamer sensors.

3.6 The integration of MN and MMP-9 aptamer sensor

As a proof of concept, an MN array was integrated with the MMP-9 aptamer sensor to evaluate the practical performance of the device (Figure 5A). In this configuration, the disposable integrated device consists of a porous MN array for tear collection, and an L-shaped sensor for biomarker detection (Figure S4). The MN array (1 × 10), prepared as described in our previous work, is porous, soft, and compatible with the ocular surface. Its aligned microchannels enable rapid tear extraction through capillary action while showing high biomarker recovery efficiency (Figure 5B to 5D).[8] After recording the baseline measurement, the MN patch is temporarily affixed to the sensor surface using a double-sided medical adhesive deposited within the predefined indentations

View Article Online
DOI: 10.1039/D6LC00230G

(Figures S5A & S5B). During use, tear fluid is first collected from the ocular surface with the MN on the integrated device (Video S1, Figure 5B & S5C). As the liquid travels from the tips to the base of the MN, tear biomarkers come into contact and interact with the aptamer-functionalized sensing interface (Figure S5D). The device is then immersed in $Fe(CN)_6^{3-/4-}$ buffer, where the medical tape loses adhesion and the MN array detaches (Figure S5E). Finally, electrochemical quantification is carried out (Figure S5F). This detachable design allows tear collection and sensing to be carried out in a single workflow while ensuring minimal sample loss, providing a user-friendly disposable biosensor.

An ocular surface agarose gel model was used for *in vitro* assessment of the integrated device (Figure 5A).[11] Commercial artificial tears spiked with 10-50 pg/mL human recombinant MMP-9, mimicking the tear states of healthy eye and dry eye (HE and DE), were loaded onto an agarose gel eye model. The baseline SWV response of the MMP-9 aptamer sensor has been pre-recorded in $Fe(CN)_6^{3-/4-}$ buffer before integration the MN patch onto the MMP-9 aptamer sensor. The MN array on the integrated device was placed on the agarose gel for 3 min, during which artificial tears was extracted through capillary-driven absorption. After collection, the device was immersed in $Fe(CN)_6^{3-/4-}$ buffer to enable MN detachment, and was left for 15 min to allow for sufficient incubation time on the sensing interface (Video S2). Then, SWV measurements were performed. The obtained responses were converted to quantitative concentrations and were fitted to a standard curve with the equation: $\Delta i/i_0 = 0.007869 * C_{MMP\text{-}9} + 0.1653$, and an R^2 of 0.86 (Figure 5D & 5E). Although the response was dampened when tested in artificial tears, presumably from the viscosity agents and other ingredients that could hinder electron transfer, the trend of the calibration curve mostly matched the standard results obtained previously.[20] Two additional artificial tear samples with 20 ng/mL and 50 ng/mL MMP-9 were prepared to represent tears from

View Article Online
DOI: 10.1039/D6LC00230G

HE and DE respectively (Figure 5F). The same collection-to-detection workflow was applied to measure the SWV responses of the samples. Based on the relative peak-current difference, the theoretical concentrations were calculated using the previously calibrated equation. For the HE sample, the measured $\Delta i/i_0$ was 0.295, leading to a theoretical concentration of 16.5 ng/mL. In the DE sample, a theoretical concentration of 46.9 ng/mL was calculated from the measured $\Delta i/i_0$, 0.535. Compared to the actual concentrations of 20 ng/mL and 50 ng/mL, the accuracy is around 85–90 % While the accuracy of the MN-integrated sensor could be further improved, the results demonstrated the practicality of detecting HE and DE tears.

These *in vitro* experiments illustrated that even in a physiologically relevant model, the integrated porous MN and aptamer sensor platform can successfully collect and quantify MMP-9 in tears, supporting its potential for DED tear biomarker detection.

View Article Online
DOI: 10.1039/D6LC00230G

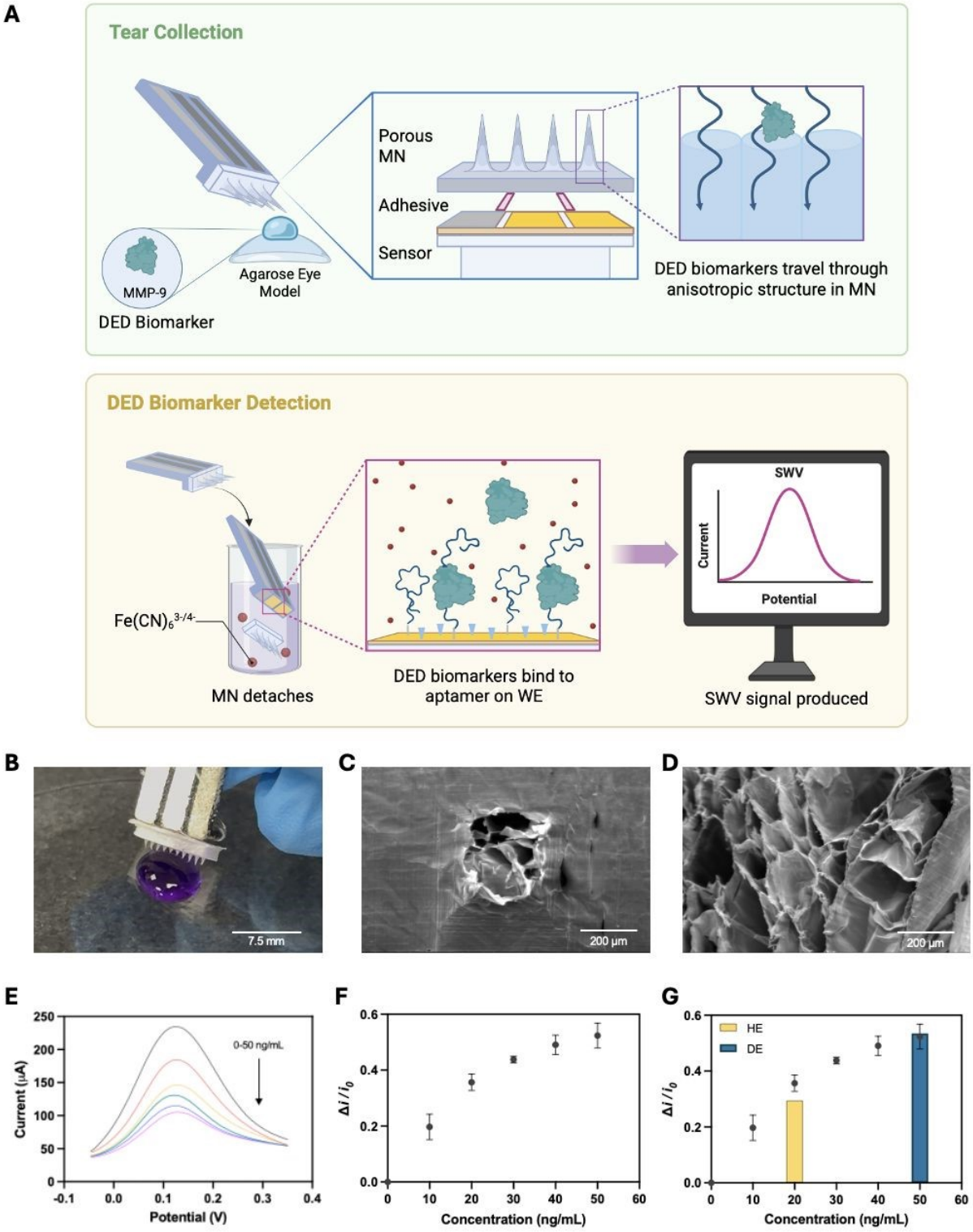

View Article Online
DOI: 10.1039/D6LC00230G

Figure 5. MN-integrated MMP-9 sensor device performance *in vitro*. (A) Schematic illustration of the workflow of the integrated device; (B) Digital image of MN collecting liquid dye, scale bar: 7.5 mm; (C) SEM image of the internal microstructure of APC-MN; (D) SEM image of the cross section of APC-MN, scale bar: 200 μm; (E) SWV of the integrated MMP-9 sensor device; (F) Calibration curve of MMP-9 sensor device using artificial tear; (G) Measurements of simulated HE and DE artificial tear samples compared to the calibration curve.

4. Conclusion

This work developed an MN-integrated electrochemical-based aptamer sensor for the detection of three dry eye disease biomarkers, IFN-γ, TNF-α, and MMP-9. In this disposable device, a soft, porous MN patch with aligned microchannels functions as the tear extraction tool for the collection of tears from the ocular surface to the sensing interface. The sensing module consists of a three-electrode system made with Au leaf, and thiolated aptamers that were attached through self-assembly. $Fe(CN)_6^{3-/4-}$ were utilized as redox probes to reflect the decrease in faradic current using SWV as the aptamers bind to their target analytes. All three sensors were able to achieve a low LOD, specifically 4.46 pg/mL, 1.56 pg/mL, and 4.97 ng/mL for IFN-γ, TNF-α, and MMP-9 respectively, in addition to a linear range that covers the clinical concentrations (13 pg/mL of IFN-γ, 4 pg/mL of TNF-α, and > 40 ng/mL of MMP-9) for DED diagnosis. The aptamer sensors also demonstrated high selectivity, as well as good anti-interference performance in the presence of common tear components. As a proof of concept, the MMP-9 aptamer sensor was integrated with a porous MN patch for the collection and detection of MMP-9 in artificial tears, illustrating the complete workflow of this integrated system *in vitro*. While there are limitations in accuracy and

View Article Online
DOI: 10.1039/D6LC00230G

quantification of tear volume, this disposable MN integrated device provides a promising direction for the point-of-care quantitative monitoring of DED.

5. Acknowledgements

C.X. appreciates the supports from Research Impact Fund (R4020-22), and General Research Fund (GRF) from the Research Grants Council (RGC) of the Hong Kong Special Administrative Region, China (CityU11202021, CityU11202222, CityU11100323, CityU 11101324), National Science Fund for Distinguished Young Scholars from National Natural Science Foundation of China (T2425004).

Conflict of interest

The authors declare no conflict of interest.

References

1. Craig, J. P. *et al.* TFOS DEWS II Definition and Classification Report. *Ocul. Surf.* **15**, 276–283 (2017).
2. Britten-Jones, A. C. *et al.* Epidemiology and Risk Factors of Dry Eye Disease: Considerations for Clinical Management. *Medicina (Mex.)* **60**, 1458 (2024).
3. Stapleton, F., Velez, F. G., Lau, C. & Wolffsohn, J. S. Dry eye disease in the young: A narrative review. *Ocul. Surf.* **31**, 11–20 (2024).
4. Kumar, N. R. *et al.* Tear biomarkers in dry eye disease: Progress in the last decade. *Indian J. Ophthalmol.* **71**, 1190–1202 (2023).

View Article Online
DOI: 10.1039/D6LC00230G

5. Lu, Z. *et al.* Rapid and quantitative detection of tear MMP-9 for dry eye patients using a novel silicon nanowire-based biosensor. *Biosens. Bioelectron.* **214**, 114498 (2022).
6. Wang, Z. *et al.* Towards detection of biomarkers in the eye using an aptamer-based graphene affinity nanobiosensor. *Talanta* **250**, 123697 (2022).
7. Mejía-Salgado, G. *et al.* Real-world performance of the inflammadry test in dry eye diagnosis: an analysis of 1,515 patients. *Graefes Arch. Clin. Exp. Ophthalmol.* **263**, 1623–1631 (2025).
8. Hu, T. *et al.* Microneedles with an anisotropic porous microstructure facilitate the transdermal delivery of small molecules, lipid nanoparticles, and T cells. *Matter* **8**, 102038 (2025).
9. Fischer, L. M. *et al.* Gold cleaning methods for electrochemical detection applications. *Microelectron. Eng.* **86**, 1282–1285 (2009).
10. Liu, Y., Tuleouva, N., Ramanculov, E. & Revzin, A. Aptamer-Based Electrochemical Biosensor for Interferon Gamma Detection. *Anal. Chem.* **82**, 8131–8136 (2010).
11. Cui, M. *et al.* Ocular Delivery of Predatory Bacteria with Cryomicroneedles Against Eye Infection. *Adv. Sci.* **8**, 2102327 (2021).
12. Santos, M. S. F., Ameku, W. A., Gutz, I. G. R. & Paixão, T. R. L. C. Gold leaf: From gilding to the fabrication of disposable, wearable and low-cost electrodes. *Talanta* **179**, 507–511 (2018).
13. Jackson, D. C. *et al.* Tear Interferon-Gamma as a Biomarker for Evaporative Dry Eye Disease. *Investig. Opthalmology Vis. Sci.* **57**, 4824 (2016).
14. Yoon, K.-C., Jeong, I.-Y., Park, Y.-G. & Yang, S.-Y. Interleukin-6 and Tumor Necrosis Factor-α Levels in Tears of Patients With Dry Eye Syndrome. *Cornea* **26**, 431–437 (2007).
15. Liu, Y., Zhou, Q. & Revzin, A. An aptasensor for electrochemical detection of tumor necrosis factor in human blood. *The Analyst* **138**, 4321 (2013).

View Article Online
DOI: 10.1039/D6LC00230G

16. Safar, W., Azziz, A., Edely, M. & Lamy De La Chapelle, M. Conventional Raman, SERS and TERS Studies of DNA Compounds. *Chemosensors* **11**, 399 (2023).

17. Signal-On Architecture for Electrochemical Aptasensors Based on Multiple Ion Channels. *ACS Publications* https://pubs.acs.org/doi/pdf/10.1021/ac302351n (2012).

18. Chen, Z., Li, H., Xie, M., Zhao, F. & Han, S. Label-Free Electrochemical Aptasensor for Sensitive Detection of Malachite Green Based on AuNPs/MWCNTs@TiO2 Nanocomposites. *Int. J. Mol. Sci.* **24**, 10594 (2023).

19. Ritz, A. J., Stuehr, O. M., Comer, D. N. & Lazenby, R. A. Controlling Gold Morphology Using Electrodeposition for the Preparation of Electrochemical Aptamer-Based Sensors. *ACS Appl. Bio Mater.* **7**, 1925–1935 (2024).

20. Galek, P., Slesinski, A., Fic, K. & Menzel, J. Peculiar role of the electrolyte viscosity in the electrochemical capacitor performance. *J. Mater. Chem. A* **9**, 8644–8654 (2021).

View Article Online
DOI: 10.1039/D6LC00230G

Data availability statements

Data for this article, including electrochemical data, original EDS and Raman spectroscopy data are available at Science Data Bank at https://10.57760/sciencedb.30014.